

Hartree–Fock Critical Nuclear Charge in Two-Electron Atoms

Hugh G. A. Burton^{1, a)}

Physical and Theoretical Chemistry Laboratory, Department of Chemistry, University of Oxford, South Parks Road, Oxford, OX1 3QZ, U.K.

(Dated: 8 January 2021)

Electron correlation effects play a key role in stabilising two-electron atoms near the critical nuclear charge, representing the smallest charge required to bind two electrons. However, deciphering the importance of these effects relies on fully understanding the uncorrelated Hartree–Fock description. Here, we investigate the properties of the ground state wave function in the small nuclear charge limit using various symmetry-restricted Hartree–Fock formalisms. We identify the nuclear charge where spin-symmetry breaking occurs to give an unrestricted wave function that predicts the ionisation of an electron. We also discover another critical nuclear charge where the closed-shell electron density detaches from the nucleus, and identify the importance of fractional spin errors and static correlation in this limit.

I. INTRODUCTION

How much positive charge is required to bind two electrons to a nucleus? This simple question has been subject to intense research and debate ever since the early 1930s.^{1–9} High-precision calculations have only recently converged on a critical nuclear charge for binding two electrons of $Z_c = 0.911\,028\,224\,077\,255\,73(4)$.^{7–9} For $Z > Z_c$, the two-electron atom ($Z e e$) is bound and stable, with an energy lower than the ionised system ($Z e + e$). However, for $Z < Z_c$, the energy of the bound atom becomes higher than the ionised system, causing an electron to spontaneously detach from the nucleus. As a result, the critical charge marks the threshold for stability in the three-body problem^{6,10,11} and can be interpreted as a quantum phase transition.¹²

While the critical nuclear charge is fascinating in its own right, the two-electron atom also provides an essential model for understanding the performance of electronic structure approximations. It is the simplest chemical system where electron correlation is present, which is thought to be essential in binding the two electrons near Z_c .^{3,13,14} In particular, comparing the closed-shell HF energy to the exact energy of the ionised system shows that HF theory fails to predict a stable two-electron atom with $Z_c < Z < 1.031\,177\,528$,¹³ including H^- .^{15,16} However, interpreting exactly *how* correlation influences the stability of the two-electron atom is made difficult by an incomplete understanding of the HF approximation for small Z .

In many ways, placing artificial restrictions on the wave function makes the HF description more complicated to interpret than the exact result. For example, the restricted HF (RHF) formalism can only predict doubly-occupied orbitals,¹⁷ and one might ask if comparing the RHF energy to the exact one-electron energy is a fair way to identify the RHF critical charge. Alternatively, the unrestricted HF (UHF) approach allows the spin-up and spin-down electrons to occupy different spatial orbitals,¹⁷ providing a qualitatively correct model for the dissociation of a single bound electron in H^- at the expense of broken spin-symmetry.^{15,16} The onset of HF symmetry breaking is marked by instability thresholds in the orbital

Hessian,¹⁸ which have also been interpreted as critical charges in closed-shell atoms.¹⁹ These sudden qualitative changes in the HF wave function can also be probed using the average radial electronic positions, providing an alternative indicator for electron ionisation that does not rely on energetic comparisons with the exact result. However, to the best of our knowledge, the exact nuclear charge for UHF symmetry breaking, and the qualitative properties of HF wave functions near this point, remain unknown.

Previous studies on the two-electron atom using HF theory have primarily focussed on the large Z , or “high-density”, limit (see e.g., Ref. 20). In this limit, the closed-shell RHF wave function provides a good approximation to the exact result, creating a model for understanding dynamic correlation.^{20,21} Alternatively, the small- Z “low-density” limit, where static correlation becomes significant, remains far less explored. The primary challenges of small Z include the presence of HF symmetry-breaking and convergence issues that occur with diffuse basis functions. One recent HF study has been unable to reliably converge the RHF approximation for $Z < 0.85$,¹³ hindering attempts to understand HF theory for smaller Z . Consequently, the small- Z limit also provides a model for understanding how to predict strong static correlation,²² which remains a major computational challenge.

In this contribution, we investigate the properties of the RHF and UHF ground-state wave functions in the small Z limit. We use numerical Laguerre-based HF calculations to compute the exact location of the UHF symmetry-breaking threshold. By investigating the average radial positions in the RHF and UHF wave functions, we assess how each HF formalism predicts electron detachment near the critical charge. Our results suggest that the UHF symmetry-breaking threshold represents the onset of ionisation and forms a branch point singularity in the complex Z plane. Alternatively, RHF theory predicts a closed-shell critical point where half the electron density becomes ionised, leading to strong static correlation for small Z .

^{a)}Electronic mail: hugh.burton@chem.ox.ac.uk

II. TWO-ELECTRON ATOMIC HAMILTONIAN

The Z -scaled Hamiltonian for the two-electron atom with an infinite nuclear mass is¹

$$\mathcal{H} = -\frac{1}{2}(\nabla_1^2 + \nabla_2^2) - \frac{1}{\rho_1} - \frac{1}{\rho_2} + \frac{1}{Z} \frac{1}{\rho_{12}}, \quad (1)$$

where $\rho_i = r_i/Z$ is the scaled distance of electron i from the nucleus, $\rho_{12} = |\rho_1 - \rho_2|$ is the scaled inter-electronic distance, and the unscaled distances have atomic units a_0 . Nuclear charges are given in atomic units e . The exact wave function is defined by the time-independent Schrödinger equation

$$\mathcal{H}\Psi(\mathbf{x}_1, \mathbf{x}_2) = \tilde{E}\Psi(\mathbf{x}_1, \mathbf{x}_2) \quad (2)$$

with the spin-spatial coordinate $\mathbf{x}_i = (\rho_i, \sigma_i)$ and the scaled energy $\tilde{E} = E/Z^2$. The electron-electron repulsion can be considered as a perturbation to the independent-particle model with the coupling strength $\lambda = 1/Z$,¹ giving the power series expansions $\tilde{E}(\lambda) = \sum_{k=0}^{\infty} \tilde{E}^{(k)} \lambda^k$ and $\Psi(\lambda) = \sum_{k=0}^{\infty} \Psi^{(k)} \lambda^k$. The critical nuclear charge Z_c can then be identified from the radius of convergence of these series,^{2,4,5,23} defined by the distance of the closest singularity to the origin in the complex λ plane.²⁴ Both $E(\lambda)$ and $|\Psi(\lambda)|^2$ have complicated singularities on the positive real axis at $\lambda_c = 1/Z_c$,⁵ which have been interpreted as a quantum phase transition in the complete-basis-set limit.¹²

The HF wave function is a single Slater determinant $\Psi_{\text{HF}}(\mathbf{x}_1, \mathbf{x}_2)$ built from the antisymmetrised product of the occupied spin-orbitals $\psi_i(\mathbf{x})$. These orbitals are self-consistent eigenfunctions of the one-electron Fock operator $\hat{f}(\mathbf{x})$, with the corresponding eigenvalues defining orbital energies. The Z -scaled Fock operator is

$$\hat{f}(\mathbf{x}) = \hat{h}(\mathbf{x}) + \frac{1}{Z} \sum_{i=1}^2 [\hat{f}_i(\mathbf{x}) - \hat{K}_i(\mathbf{x})], \quad (3)$$

with the one-electron Hamiltonian

$$\hat{h}(\mathbf{x}) = -\frac{\nabla^2}{2} - \frac{1}{\rho}, \quad (4)$$

and the Coulomb and exchange operators denoted as $\hat{f}_i(\mathbf{x})$ and $\hat{K}_i(\mathbf{x})$ respectively (see Ref. 17). The total HF energy is

$$\tilde{E}^{\text{HF}} = \frac{1}{2} \sum_{i=1}^2 (h_i + f_i), \quad (5)$$

with the matrix elements $h_i = \langle \psi_i | \hat{h} | \psi_i \rangle$ and $f_i = \langle \psi_i | \hat{f} | \psi_i \rangle$.

The self-consistent two-electron component of the Fock operator can be considered as a perturbation with the coupling strength $\lambda = 1/Z$. For large Z ($\lambda \rightarrow 0$), only the one-electron component remains and the HF wave function is exact.²⁰ As Z becomes smaller and λ grows, the self-consistent repulsion becomes increasingly dominant over the one-electron nuclear attraction. Eventually, it becomes energetically favourable for a pair of lower-energy UHF solutions to emerge where either the spin-up or spin-down electron becomes detached from the

nucleus.^{15,16} This phenomenon is analogous to the Coulson–Fischer point in stretched H_2 , where the spin-up and spin-down electrons localise on opposite atoms,²⁵ and is closely related to Wigner crystallisation.²⁶ By analytically continuing an equivalent two-electron coupling parameter to complex values, we have recently shown that the UHF wave functions form a non-Hermitian square-root branch point at the symmetry-breaking threshold.^{24,27} Remarkably, following a complex-valued contour around this point leads to the interconversion of the degenerate solutions, and allows a ground-state wave function to be smoothly evolved into an excited-state wave function.²⁷

III. COMPUTATIONAL DETAILS

In the present work, we follow Ref. 13 and express the spatial component $\phi_p(\mathbf{r})$ of the HF spin-orbital $\psi_p(\mathbf{x})$ using the spherically-symmetric Laguerre-based functions²⁸

$$\chi_\mu(\mathbf{r}) = \exp\left(-\frac{Ar}{2}\right) L_\mu^{(1)}(Ar), \quad (6)$$

giving

$$\phi_p(\mathbf{r}) = \sum_{\mu=0}^{\infty} \chi_\mu(\mathbf{r}) C_{\mu,p}^{\mu}. \quad (7)$$

Here we employ the nonorthogonal tensor notation of Head–Gordon *et al.*²⁹ The non-linear parameter A controls the spatial extent of the basis functions and is optimised alongside the coefficients $C_{\mu,p}^{\mu}$.¹³ In practice, this expansion is truncated at a finite basis set of size n . To avoid previous issues with iterative solutions to the HF equations for small Z , we optimise the $C_{\mu,p}^{\mu}$ coefficients for a fixed A value using the quasi-Newton Geometric Direct Minimisation (GDM) algorithm.³⁰ The optimal A value is then identified through another quasi-Newton minimisation with the orbital coefficients re-optimised on each step. All calculations were performed in a developmental version of Q-CHEM,³¹ and analytic expressions for the Laguerre-based integrals are provided in the Supporting Information.

IV. RESULTS

A. Spin-Symmetry Breaking Critical Point

First, we identify the critical nuclear charge for HF symmetry-breaking Z_c^{UHF} using a bisection method to locate the point where the lowest orbital Hessian eigenvalue of the RHF solution vanishes.¹⁸ The convergence of Z_c^{UHF} with respect to the basis set size is shown in Table I, giving a best estimate of $Z_c^{\text{UHF}} = 1.057\,660\,253\,46(1)$. This value is converged for $n \geq 24$, for which converged RHF energies for He and H^- are also obtained as

$$E_{\text{RHF}}(\text{He}) = -2.861\,679\,995\,612\,23(1)$$

$$E_{\text{RHF}}(\text{H}^-) = -0.487\,929\,734\,370\,84(1),$$

in agreement with the best variational benchmarks up to 10 decimal places.^{13,32,33} We believe that this is the first numerically precise estimate of a symmetry-breaking threshold in the complete-basis-set HF limit, and therefore defines a new type of benchmark value within electronic structure theory. As expected, we find $Z_c^{\text{UHF}} > 1$, and thus our result is consistent with previous observations of UHF symmetry breaking in the hydride anion.^{15,16}

TABLE I: Convergence of the UHF symmetry-breaking threshold Z_c^{UHF} and the associated energy $E^{\text{UHF}}(Z_c^{\text{UHF}})$ with respect to basis set size. Best estimates and quoted errors correspond to the mean and standard deviation of the converged values $n \geq 24$ respectively.

n	Z_c^{UHF}/e	$E^{\text{UHF}}(Z_c^{\text{UHF}})/E_h$
10	1.057 651 800 057	-0.570 335 516 87
12	1.057 658 412 462	-0.570 345 373 24
14	1.057 659 966 054	-0.570 347 687 12
16	1.057 660 213 291	-0.570 348 055 22
18	1.057 660 248 206	-0.570 348 107 19
20	1.057 660 252 818	-0.570 348 114 05
22	1.057 660 253 391	-0.570 348 114 91
24	1.057 660 253 461	-0.570 348 115 01
26	1.057 660 253 464	-0.570 348 115 01
28	1.057 660 253 462	-0.570 348 115 01
30	1.057 660 253 464	-0.570 348 115 02
32	1.057 660 253 439	-0.570 348 114 98
34	1.057 660 253 473	-0.570 348 115 03
36	1.057 660 253 458	-0.570 348 115 01
38	1.057 660 253 477	-0.570 348 115 03
40	1.057 660 253 466	-0.570 348 115 02
Best	1.057 660 253 46(1)	-0.570 348 115 01(2)

Figure 1 (top panel) compares the Z -scaled RHF energy (red) and the symmetry-broken UHF energy (blue dashed) as functions of Z^{-1} with $n = 26$. We also consider the exact one-electron energy (black) that corresponds to the ionised atom, the exact two-electron energy (grey dashed; reproduced from Ref. 8), and a fractional spin RHF calculation (dashed orange) with half a spin-up and half spin-down electron (see Sec. IV C). The UHF symmetry-breaking threshold Z_c^{UHF} (black dot) occurs below the exact one-electron energy, and thus Z_c^{UHF} is greater than the HF critical nuclear charge previously identified using energetic arguments.¹³ This suggests that the RHF approximation is already an inadequate representation of the exact wave function before it becomes degenerate with the one-electron atom. Beyond this point, the RHF energy continues to increase, while the UHF energy rapidly flattens towards the exact one-electron result. There is therefore a small relaxation region during which the UHF approximation approaches a qualitative representation of the one-electron atom.

Radial electron position expectation values $\langle r \rangle$ provide further insights into the properties of the two-electron atom close to electron detachment.^{8,14,34} The exact wave function yields an “inner” and “outer” electron, with repulsive interactions pushing the inner electron closer to the nucleus than in the corresponding hydrogenic system.³⁴ For $Z > Z_c^{\text{UHF}}$, the RHF radial electron position closely matches the averaged exact

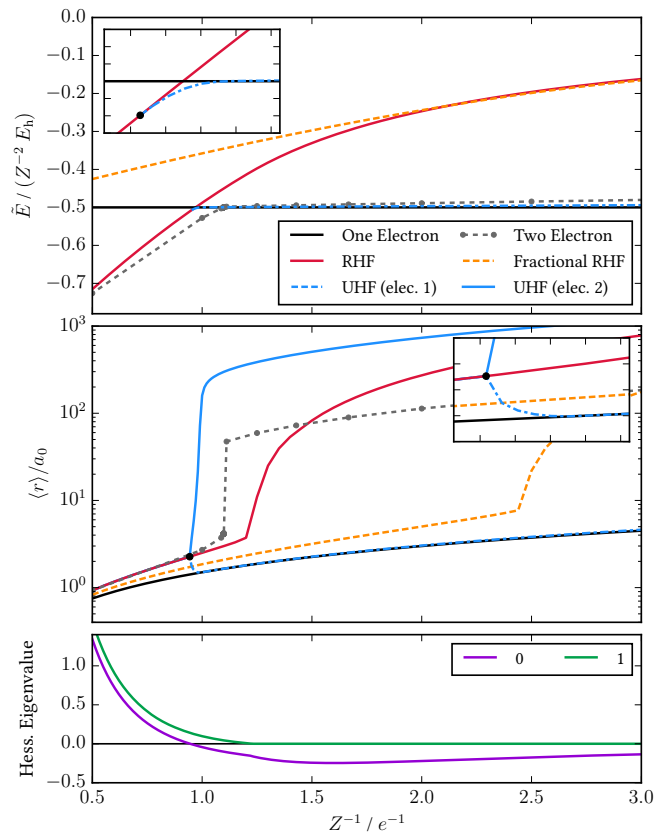


FIG. 1: Z -scaled energy (top) and average radial position $\langle r \rangle$ (middle) using various HF formalisms and exact one- and two-electron results. Exact two-electron data are reproduced from Ref. 8. The lowest two Hessian eigenvalues for the RHF solution (bottom) show the onset of UHF symmetry breaking and a persistent zero eigenvalue for small Z .

two-electron result (grey dashed). However, the RHF result starts to deviate from the two-electron value as electron correlation effects become significant for $Z < Z_c^{\text{UHF}}$. In contrast, the additional flexibility of the UHF wave function correctly predicts the separation of an inner and outer electron. This ionisation occurs almost immediately for $Z < Z_c^{\text{UHF}}$, as indicated by a sudden increase in $\langle r \rangle$ for the dissociating electron (Fig. 1: middle panel), while the bound electron tends towards the exact one-electron result. Comparing the radial distribution functions $P(r) = r^2|\psi(r)|^2$ for each electronic orbital at $Z = 1$ (Fig. 2), we find that the inner UHF orbital closely matches the one-electron H atom, which is also the case for the exact wave function.³⁴ However, at $Z = 1$, the outer electron has essentially ionised from the atom in the UHF approximation, but remains closely bound to the nucleus in the fully-correlated description. The UHF wave function therefore rapidly approximates the ionised atom for $Z < Z_c^{\text{UHF}}$, and Z_c^{UHF} can be interpreted as a critical charge for a stable two-electron atom. This approximation essentially overlocalises the electron density between $Z_c < Z < Z_c^{\text{UHF}}$ (including H^-), as previously observed for two-electrons on concentric spheres,³⁵ and fails to capture the correlation required to describe the exact critical charge.

Figure 1 also indicates that the dissociation of the outer elec-

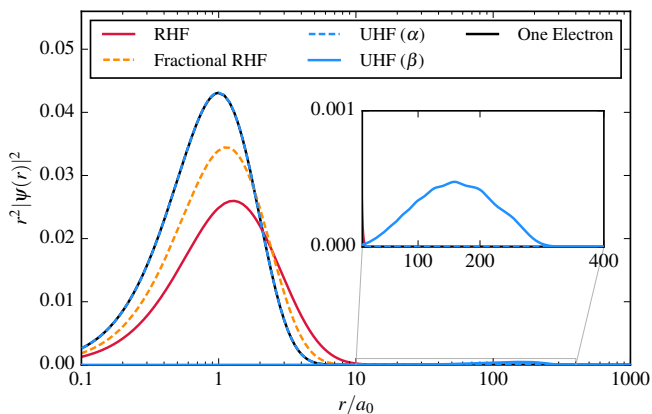


FIG. 2: Radial distribution functions for different HF orbitals compared to the exact one-electron wave function at $Z = 1$.

tron for the UHF approximation is relatively sudden and closely mirrors the behaviour at the exact critical nuclear charge.⁸ Furthermore, there is small region where the average radial position of the inner electron tends towards the one-electron result. It is known that the exact two-electron system exhibits a shape resonance as the nuclear charge goes through the critical point, with the outer electron remaining at a finite distance from the nucleus.^{7,36} One might therefore interpret the region where the UHF electron positions tend towards the one-electron result as an approximation of this resonant stability regime.

For $Z < Z_c$, the exact wave function is an equal combination of two configurations where either the spin-up or spin-down electron remains bound to the nucleus. In contrast, the single-determinant nature of the UHF wave function means that only one of these configurations can be represented: the UHF orbitals are “pinned” to one resonance form.³⁷ There must therefore be a wave function singularity at Z_c^{UHF} where the UHF approximation branches into a form with either the spin-up or spin-down electron remaining bound. The mathematical structure of this point can be revealed by following a continuous pathway around Z_c^{UHF} in the complex Z plane. When Z is analytically continued to complex values, the Fock operator becomes non-Hermitian and we must consider the holomorphic HF approach.^{38–40} In the remainder of this Section, we fix the non-linear A parameter to its value at Z_c^{UHF} as the non-Hermitian energy is complex-valued and cannot be variationally optimised.

Figure 3 shows the real component of $\langle r \rangle$ for the (initial) inner electron along a pathway which spirals in towards Z_c^{UHF} , parametrised as

$$Z(\xi) = Z_c^{\text{UHF}} - \left(0.02 - \frac{0.001\xi}{2\pi}\right) \exp(i\xi). \quad (8)$$

Remarkably, after one complete rotation ($\xi = 2\pi$), the inner and outer electrons have swapped, indicating that the degenerate UHF solutions have been interconverted. A second full rotation is required to return the states to their original forms. The two degenerate UHF wave functions are therefore connected as a square-root branch point in the complex- Z plane, in agreement with our previous observations in analytically solvable models.^{24,27} Furthermore, the branch point behaves

as a quasi-exceptional point, where the two solutions become identical but remain normalised (see Ref. 27), providing the first example of this type of non-Hermitian HF degeneracy in the complete-basis-set limit.

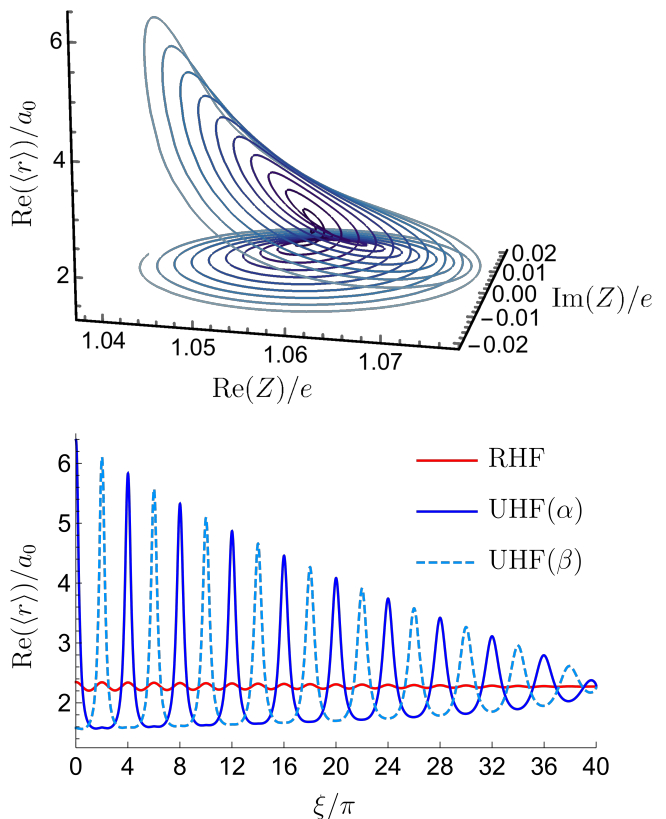


FIG. 3: Average radial position $\langle r \rangle$ of the inner electron along a spiral contour in the complex Z plane converging on Z_c^{UHF} using $n = 26$. On each rotation, the UHF wave function transitions between the two degenerate solutions.

B. Closed-Shell Critical Point

We now consider the fate of the RHF ground state as Z continues to decrease below Z_c^{UHF} . Intuitively, one might expect that the doubly-occupied RHF orbitals would be unable to describe the open-shell atom with an ionised electron. Indeed, King *et al.* have observed a smooth and finite $\langle r \rangle$ value for the RHF wave function as low as $Z = 0.85$, with erratic convergence for lower nuclear charges.¹³ A similar nuclear charge $Z = 0.84$ was identified in Ref. 19 as a singlet instability threshold, where the orbital Hessian contains a zero eigenvalue with respect to symmetry-pure orbital rotations. These observations suggest that the RHF approximation somehow breaks down at $Z \approx 0.84$, but we are not aware of any detailed insight into this behaviour.

By using the gradient-based GDM algorithm,³⁰ we have accurately converged the RHF ground state for all nuclear charges

and can now firmly establish its properties in the small- Z limit. Remarkably, we find a sudden increase in $\langle r \rangle$ at $Z_c^{\text{RHF}} = 0.82$ (Fig. 1: middle panel) suggesting that the RHF approximation can, to a certain extent, represent the ionised system. This feature closely mirrors the electron dissociation in the UHF wave function, but gives a less sudden increase. The smoother nature of the RHF dissociation indicates that the closed-shell restriction on the orbitals artificially attenuates the electron detachment, providing a less accurate representation of the exact critical charge than the UHF description.

The RHF electron detachment is accompanied by the onset of another zero eigenvalue in the orbital Hessian, as described in Ref. 19, but we find that this persists for small Z (Fig. 1: bottom panel). Zero Hessian eigenvalues generally indicate a broken continuous symmetry in the wave function, such as a global spin-rotation,^{41,42} and define the so-called ‘‘Goldstone’’ manifold of degenerate states.^{42,43} In this instance, the new zero-eigenvalue Hessian mode corresponds to a spin-symmetry-breaking orbital rotation that also leads to an ‘‘inner’’ and ‘‘outer’’ electron. Since the energy is constant along this mode, this additional zero Hessian eigenvalue suggests that the RHF approximation has become unstable with respect to electron detachment. Consequently, the sudden increase in $\langle r \rangle$ at Z_c^{RHF} qualitatively represents a closed-shell critical nuclear charge at $Z_c^{\text{RHF}} = 0.82$.

To further understand the electron positions in the vicinity of Z_c^{RHF} , we consider the cumulative radial distribution function of the doubly-occupied RHF orbital

$$N_{\text{RHF}}(r) = \int_0^{2\pi} \int_0^\pi \int_0^r |\psi_{\text{RHF}}(r')|^2 r'^2 \sin \theta dr' d\theta d\phi, \quad (9)$$

as shown in Fig. 4. The single-step structure at $Z > Z_c^{\text{RHF}}$ and is consistent with a single peak in the radial distribution function (see e.g. Fig. 2), indicating that the electrons are closely bound to the nucleus. For $Z < Z_c^{\text{RHF}}$, this cumulative density

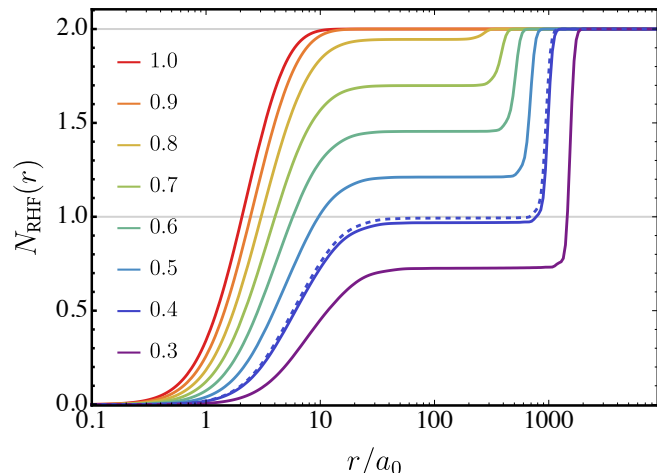


FIG. 4: Cumulative radial distribution function for the RHF wave function using $n = 26$. For $Z < 0.82$, this function adopts a double-step structure corresponding to an inner and outer peak in the radial electron density. At $Z = 0.41$, each peak contains half the electron density (dashed line).

adopts a double-step structure corresponding to a radial density peak close to the nucleus, and another representing an unbound electron. The magnitude of the second step continues to grow for smaller Z as the outer peak becomes increasingly unbound until, at $Z = 0.41$, the inner and outer peaks both contain exactly one electron. For smaller Z , all the electron density becomes unbound. Remarkably, the RHF wave function for $0.41 < Z < Z_c^{\text{RHF}}$ is therefore providing a closed-shell representation of the open-shell atom by delocalising the electron density over the bound and unbound radial ‘‘sites’’. This delocalisation allows the RHF wave function to provide a qualitatively correct representation of the exact one-body density, but fails to capture any two-body correlation between the bound and unbound electrons.

C. Fractional Spin Error

Although the RHF radial density for $Z < Z_c^{\text{RHF}}$ appears to be approximating the exact result, the RHF energy remains consistently above the one-electron hydrogenic energy. The closed-shell nature of the RHF orbitals means that the inner and outer radial density peaks both contain half a spin-up electron and half a spin-down electron bound to the nucleus. As a result, the RHF electron distribution for small Z tends towards a description of the one-electron atom that also contains half a spin-up and half a spin-down electron. We have confirmed this limiting behaviour by computing the RHF energy with a half-occupied orbital, also known as the ‘‘spin-unpolarised’’ atom with fractional spins.^{44–46} As expected, this half-occupied RHF solution becomes degenerate with the two-electron RHF energy at small Z (Fig 1: top panel).

Remarkably, even though a one-electron atom always has a bound ground state, we find that the fractional spin RHF wave function predicts an additional critical nuclear charge at $Z_c^{\text{frac}} = 0.41$, where the (half) electrons suddenly become unbound (Fig 1: middle panel). This critical charge matches the point where half the electron density has ionised from the nucleus in the conventional RHF approach (dashed line in Fig. 4). It is well-known that RHF with fractional spins fails to predict the correct energy for one-electron atoms, despite the fact that HF theory should be exact in this limit, and causes the static correlation error that leads to the RHF breakdown for stretched H_2 .^{44,45} We therefore conclude that this static correlation also creates an artificial critical nuclear charge in one-electron atoms at $Z_c^{\text{frac}} = 0.41$, and is responsible for the failure of conventional RHF in the small Z limit. Identifying similar artificial critical charges using a density functional approximation would almost certainly provide new insights into the failures of such methods for anionic energies and electron affinities.^{47–49}

V. CONCLUDING REMARKS

In summary, we have used average radial electronic positions to understand where HF theory predicts electron detachment in the two-electron atom, providing alternative critical nuclear

charges in the RHF and UHF formalisms. For UHF theory, this critical charge corresponds to a spin-symmetry-breaking threshold $Z_c^{\text{UHF}} = 1.057\,660\,253\,46(1)$ where one electron suddenly ionises from the nucleus. In contrast, at the RHF critical charge $Z_c^{\text{RHF}} = 0.82$, a secondary peak appears in the radial distribution function at large distances from the nucleus. These results provide a broader perspective on electron correlation in the small- Z limit. For example, the RHF $\langle r \rangle$ value starts to deviate from the exact two-electron result at the UHF symmetry-breaking threshold, suggesting that Z_c^{UHF} marks the onset of static correlation. This static correlation is further supported by the existence of degenerate UHF solutions representing the dominant configurations in the exact wave function. Since the UHF radial distribution functions are qualitatively incorrect for $Z_c < Z < Z_c^{\text{UHF}}$, this static correlation must be essential for binding the two-electron atom near Z_c . Furthermore, the breakdown of the half-occupied one-electron RHF result at $Z_c^{\text{frac}} = 0.41$ indicates that fractional spin errors occur for small Z , reinforcing the importance of static correlation.

For $Z < Z_c$, the exact wave function contains two dominant resonance forms with the spin-up or spin-down electron ionised from the nucleus. As the electrons are indistinguishable, the one-electron density is delocalised between the bound and unbound “sites”, and this is reflected in the RHF wave function. However, instantaneous electron-electron correlations ensure that, when one electron is bound to the nucleus, the other electron becomes unbound. UHF theory provides a snapshot of these correlations, with one electron permanently bound to the nucleus, but it cannot describe the resonance between the two sites. Alternatively, when each orbital can contain a spin-up and spin-down component in generalised HF (GHF), the symmetry-broken UHF solutions form a continuum of GHF solutions parameterised by a global spin rotation.⁴¹ The resonance between the two sites is therefore represented by this continuum, and could be computed using a (nonorthogonal) linear combination of stationary wave functions.^{50,51}

Finally, the degenerate UHF wave functions form a square-root branch point in the complex Z plane at Z_c^{UHF} . Following a continuous complex path around this point interconverts the two degenerate solutions and swaps the dissociated electron, while a second rotation returns the solutions to their original forms. We have previously observed this behaviour in analytic models, but our current results suggest that this phenomenon extends to the complete-basis-set limit.^{24,27} Furthermore, Ref. 27 shows that these complex branch points can allow a ground-state wave function to be smoothly “morphed” into an excited-state wave function by following a continuous complex contour. The two-electron atom therefore provides a new model for understanding these complex connections near the complete-basis-set limit, and we intend to continue this investigation in the future.

SUPPORTING INFORMATION

See the supporting information for analytic derivations of the Laguerre-based one- and two-electron integrals.

ACKNOWLEDGEMENTS

I gratefully thank New College, Oxford for funding through the Astor Junior Research Fellowship. I also thank Hazel Cox for providing the exact two-electron numerical data from Ref. 8, and Pierre-François Loos for countless inspiring conversations and critical comments on this manuscript.

DATA AVAILABILITY

The data that support the findings of this study are available from the author upon reasonable request.

- ¹E. A. Hylleraas, *Z. Phys.* **65**, 209 (1930).
- ²F. H. Stillinger, *J. Chem. Phys.* **45**, 3623 (1966).
- ³F. H. Stillinger and T. A. Weber, *Phys. Rev. A* **10**, 1122 (1974).
- ⁴I. A. Ivanov, *Phys. Rev. A* **51**, 1080 (1995).
- ⁵J. D. Baker, D. E. Freund, R. N. Hill, and J. D. Morgan III, *Phys. Rev. A* **41**, 1247 (1990).
- ⁶E. A. G. Armour, J.-M. Richard, and K. Varga, *Phys. Rep.* **413**, 1 (2005).
- ⁷C. S. Estienne, M. Busuttill, A. Moini, and G. W. F. Drake, *Phys. Rev. Lett.* **112**, 173001 (2014).
- ⁸A. W. King, L. C. Rhodes, C. A. Readman, and H. Cox, *Phys. Rev. A* **91**, 042512 (2015).
- ⁹H. Olivares Pilon and A. V. Turbiner, *Phys. Lett. A* **379**, 688 (2015).
- ¹⁰S. Kais and Q. Shi, *Phys. Rev. A* **62**, 060502 (2000).
- ¹¹A. W. King, F. Longford, and H. Cox, *J. Chem. Phys.* **139**, 224306 (2013).
- ¹²S. Kais, C. Wegner, and Q. Wei, *Chem. Phys. Lett.* **423**, 45 (2006).
- ¹³A. W. King, A. L. Baskerville, and H. Cox, *Phil. Trans. R. Soc. A* **376**, 20170153 (2018).
- ¹⁴A. L. Baskerville, A. W. King, and H. Cox, *R. Soc. open sci.* **6**, 181357 (2019).
- ¹⁵W. A. Goddard, *Phys. Rev.* **172**, 7 (1968).
- ¹⁶H. Cox, A. L. Baskerville, V. J. Syrjanen, and M. Melgaard, *Adv. Quantum Chem.* **81**, 167 (2020).
- ¹⁷A. Szabo and N. S. Ostlund, *Modern Quantum Chemistry* (Dover Publications Inc., 1989).
- ¹⁸R. Seeger and J. A. Pople, *J. Chem. Phys.* **66**, 3045 (1977).
- ¹⁹T. Uhlřřova and J. Zamastil, *Phys. Rev. A* **101**, 062504 (2020).
- ²⁰P.-F. Loos and P. M. W. Gill, *Chem. Phys. Lett.* **500**, 1 (2010).
- ²¹P.-F. Loos and P. M. W. Gill, *J. Chem. Phys.* **131**, 241101 (2009).
- ²²J. W. Hollett and P. M. W. Gill, *J. Chem. Phys.* **134**, 114111 (2011).
- ²³I. A. Ivanov, *Phys. Rev. A* **52**, 1942 (1995).
- ²⁴A. Marie, H. G. A. Burton, and P.-F. Loos, (2020), arXiv:2012.03688.
- ²⁵C. A. Coulson and I. Fischer, *Philos. Mag.* **40**, 386 (1949).
- ²⁶E. Wigner, *Phys. Rev.* **46**, 1002 (1934).
- ²⁷H. G. A. Burton, A. J. W. Thom, and P.-F. Loos, *J. Chem. Phys.* **150**, 041103 (2019).
- ²⁸K. F. Riley, M. P. Hobson, and S. J. Bence, *Mathematical Methods for Physics and Engineering* (Cambridge University Press, 2006).
- ²⁹M. Head-Gordon, P. E. Maslen, and C. A. White, *J. Chem. Phys.* **108**, 616 (1998).
- ³⁰T. Van Voorhis and M. Head-Gordon, *Mol. Phys.* **100**, 1713 (2002).
- ³¹Y. Shao, Z. Gan, E. Epifanovsky, A. T. Gilbert, M. Wormit, J. Kussmann, A. W. Lange, A. Behn, J. Deng, X. Feng, *et al.*, *Mol. Phys.* **113**, 184 (2015).
- ³²S. Lehtola, *Int. J. Quantum Chem.* **119**, e25945 (2019).
- ³³C. C. J. Roothaan and G. A. Soukup, *Int. J. Quantum Chem.* **15**, 449 (1979).
- ³⁴A. W. King, L. C. Rhodes, and H. Cox, *Phys. Rev. A* **93**, 022509 (2018).
- ³⁵P.-F. Loos and P. M. W. Gill, *Phys. Rev. A* **81**, 052510 (2010).
- ³⁶M. Hoffmann-Ostenhof, T. Hoffman-Ostenhof, and B. Simon, *J. Phys. A: Math. Gen.* **16**, 1125 (1983).
- ³⁷J. R. Trail, M. D. Towler, and R. J. Needs, *Phys. Rev. B* **68**, 045107 (2003).
- ³⁸H. G. Hiscock and A. J. W. Thom, *J. Chem. Theory Comput.* **10**, 4795 (2014).
- ³⁹H. G. A. Burton and A. J. W. Thom, *J. Chem. Theory Comput.* **12**, 167 (2016).

- ⁴⁰H. G. A. Burton, M. Gross, and A. J. W. Thom, *J. Chem. Theory Comput.* **14**, 607 (2018).
- ⁴¹H. G. A. Burton and D. J. Wales, *J. Chem. Theory Comput.* **XX**, XXXX (2021).
- ⁴²Y. Cui, I. W. Bulik, C. A. Jiménez-Hoyos, T. M. Henderson, and G. E. Scuseria, *J. Chem. Phys.* **139**, 154107 (2013).
- ⁴³C. A. Jiménez-Hoyos, R. R. Rodríguez-Guzmán, T. M. Henderson, and G. E. Scuseria, (2020), [arXiv:2004.05047](https://arxiv.org/abs/2004.05047).
- ⁴⁴A. J. Cohen, P. Mori-Sánchez, and W. Yang, *J. Chem. Phys.* **129**, 121104 (2008).
- ⁴⁵A. J. Cohen, P. Mori-Sánchez, and W. Yang, *Science* **321**, 792 (2008).
- ⁴⁶T. J. Daas, J. Grossi, S. Vuckovic, Z. H. Musslimani, D. P. Kooi, M. Seidl, K. J. H. Giesbertz, and P. Gori-Giorgi, (2020), [arXiv:2009.04326](https://arxiv.org/abs/2009.04326).
- ⁴⁷F. Jensen, *J. Chem. Theory Comput.* **6**, 2726 (2010).
- ⁴⁸M.-C. Kim, E. Sim, and K. Burke, *J. Chem. Phys.* **134**, 171103 (2011).
- ⁴⁹M. J. G. Peach, A. M. Teale, T. Helgaker, and D. J. Tozer, *J. Chem. Theory Comput.* **11**, 5262 (2015).
- ⁵⁰A. J. W. Thom and M. Head-Gordon, *J. Chem. Phys.* **131**, 124113 (2009).
- ⁵¹H. G. A. Burton and A. J. W. Thom, *J. Chem. Theory Comput.* **15**, 4851 (2019).